KTH Fysik

Lifetime Measurements of Excited States in ^{165}Lu and ^{107}Cd

KARIN ANDGREN

Licentiate Thesis in Physics
Stockholm, Sweden, 2006

TRITA-FYS 2006:71
ISSN 0280-316X
ISRN KTH/FYS/–06:71–SE
ISBN 91-7178-513-2, 978-91-7178-513-8

KTH Fysik
SE-100 44 Stockholm
SWEDEN

Akademisk avhandling som med tillstånd av Kungl Tekniska högskolan framlägges till offentlig granskning för avläggande av Teknologie Licentiatexamen 6 December 2006 kl 10.00 i Sal FB41, Albanova university centrum, Roslagstullsbacken 21, Stockholm.

Tryck: Universitetssevice US AB

Abstract

Measuring lifetimes of excited nuclear states can give important information on the internal structure of the nucleus. This thesis is based on two experiments performed in Italy and in the USA in order to deduce the lifetimes of excited states in ^{165}Lu and ^{107}Cd. The lifetimes were measured using the Recoil Distance Method and the reduced transition probabilities between states have been calculated from the lifetimes in a model independent way. In the analysis of the data from the experiment on ^{165}Lu, the shape of the nucleus is investigated using a collective rotational model to describe the observed excited states. A possibility of a triaxial shape of this nucleus is discussed. In the second experiment the obtained reduced transition probabilities for the nucleus ^{107}Cd are compared to theoretical predictions for vibrational and rotational excitation modes.

List of Publications

This thesis is based on the first two publications in the list below. The author's name is underlined in each case.

1. Lifetime Measurement of Normal Deformed States in $^{165}_{71}$Lu
   K. Andgren, Zs. Podolyák, A. Dewald, F.R. Xu, A. Algora, M. Axiotis, D. Bazzacco, P.G. Bizzeti, A.M. Bizzeti-Sona, B. Cederwall, G. de Angelis, E. Farnea, A. Fitzler, A. Gadea, W. Gelletly, S. Lunardi, O. Möller, N. Marginean, T. Martinez, T. Pissulla, C. Rusu, C.A. Ur, R. Venturelli, P.M. Walker and C. Wheldon
   Physical Review **C**71, 014312 (2005)

2. RDM Lifetime Measurements in ^{107}Cd
   K. Andgren, S.F. Ashley, P.H. Regan, E.A. McCutchan, N.V. Zamfir, L. Amon, R.B. Cakirli, R.F. Casten, R.M. Clark, G. Gürdal, K.L. Keyes, D.A. Meyer, M.N. Erduran, A. Papenberg, N. Pietralla, C. Plettner, G. Rainovski, R.V. Ribas, N.J. Thomas, J. Vinson, D.D. Warner, V. Werner and E. Williams
   Journal of Physics G: Nuclear and Particle Physics **31** S1563 (2005)

Other articles the author has contributed to, which are not commented on within this thesis.

1. Intrinsic State Lifetimes in ^{103}Pd and ^{106,107}Cd
   S.F. Ashley, K. Andgren, P.H. Regan, E.A. McCutchan, N.V. Zamfir, L. Amon, R.B. Cakirli, R.F. Casten, R.M. Clark, G. Gürdal, K.L. Keyes, D.A. Meyer, M.N. Erduran, A. Papenberg, N. Pietralla, C. Plettner, G. Rainovski, R.V. Ribas, N.J. Thomas, J. Vinson, D.D. Warner, V. Werner, E. Williams, H.L. Liu and F. R. Xu
   To be submitted to Physical Review **C**

2. First identification of excited states in ^{106}Te and evidence for isoscalar-enhanced vibrational collectivity
   B. Hadinia, B. Cederwall, J. Blomqvist, E. Ganioğlu, P.T. Greenlees, K. Andgren, I.G. Darby, S. Eeckhaudt, E. Ideguchi, P.M. Jones, D.T. Joss, R. Julin, S. Juutinen, S. Ketelhut, K. Lagergren, A.-P. Leppänen, M. Leino, M. Nyman,

J. Pakarinen, E.S. Paul, M. Petri, P. Rahkila, M. Sandzelius, J. Sarén, C. Scholey, J. Uusitalo, R. Wadsworth and R. Wyss
Physical Review **C** 72, 041303(R) (2005)

3. Spectroscopy of ^{212}Po and ^{213}At using a ^{8}He radioactive beam and EXOGAM
A.B. Garnsworthy, N.J. Thompson, Zs. Podolyák, P.M. Walker, S.J. Williams, G.D. Dracoulis, G. de France, G. J. Lane, K. Andgren, A.M. Bruce, A.P. Byrne, W.N. Catford, B. Cederwall, G.A. Jones, B. McGuirk, S. Mandal, E.S. Paul, V. Pucknell, N. Redon, B. Rosse, R.J. Senior and G. Sletten
Journal of Physics G: Nuclear and Particle Physics **31** S1851 (2005)

4. Vibrational and rotational sequences in ^{101}Mo and ^{103,4}Ru, studied via multinucleon transfer reactions
P.H. Regan, C. Wheldon, A.D. Yamamoto, J.J. Valiente-Dobon, D. Cline, C.Y. Wu, A.O. Macchiavelli, F.R. Xu, J.F. Smith, K. Andgren, R.S. Chakrawarthy, M. Cromaz, P. Fallon, S.J. Freeman, A. Gorgen, A. Hayes, H. Hua, S.D. Langdown, I.-Y. Lee, C.J. Pearson, Zs. Podolyák, R. Teng
Acta Physica Polonica B **36**, 1313 (2005)

5. Binary-reaction spectroscopy of ^{99,100}Mo : Intruder alignment systematics in $N = 57$ and $N = 58$ isotones
P.H. Regan, A.D. Yamamoto, F.R. Xu, C.Y. Wu, A.O. Macchiavelli, D. Cline, J.F. Smith, S.J. Freeman, J.J. Valiente-Dobón, K. Andgren, R.S. Chakrawarthy, M. Cromaz, P. Fallon, W. Gelletly, A. Gorgen, A. Hayes, H. Hua, S.D. Langdown, I-Y. Lee, C.J. Pearson, Zs. Podolyák, R. Teng, and C. Wheldon
Physical Review **C**68, 044313 (2003)

Contents

Chapter 1

Introduction

The understanding of atomic nuclei is important both on a small scale, for further knowledge on how some of the smallest building blocks in nature are constituted and on a larger scale, for understanding the development and the isotopic abundances of our universe. By examining the properties of the nuclei involved in the nucleosynthesis inside stars, conclusions can be drawn on how the elements are formed. Many different models have been developed to describe the many-body systems of atomic nuclei, from collective models (such as the liquid drop model) where the individuality of the nucleons building up the nucleus do not play any role, to the other extreme of considering the nucleus as a Fermi gas of non-interacting nucleons. Nowadays a general assumption is that the nucleons are moving independently of each other inside a mean-field potential. The interactions not taken care of by the mean field, e.g. pairing forces between like nucleons, are referred to as residual interactions. It might seem unreasonable to assume that the protons and neutrons can move freely inside such a dense object as the atomic nucleus (in the order of $\approx 10^{14}$ g/cm^3), but according to the Pauli principle two fermions are prohibited to occupy the same quantal state, thus giving the nucleons a mean-free path of the same order ($\approx 10^{-14}$ m) as the size of the nucleus. The properties of stable isotopes are well studied and to test the validity of the theoretical models used to describe these systems, experiments to produce unstable "exotic" nuclei have to be performed. The recent discoveries of neutron halos in light neutron-rich nuclei extending the radius of these nuclei far beyond the compact nuclear core, as well as superdeformation (where the nucleus behaves as an ellipsoidal object with axis ratio $\approx$ 2:1) in heavier isotopes shows the importance of further experimental studies. Such experiments with purpose of creating short-lived isotopes in exotic states, in terms of neutron to proton ratio and high angular momenta, are usually done by accelerating heavy ions onto a target with high isotope purity. The last decades' development of large γ-ray detector arrays has given us the opportunity to perform research on the structure of stable and short-lived isotopes using fusion-evaporation reactions. The experiments performed up until now have

used collisions of stable beams with stable targets. This type of reactions leads to neutron-deficient isotopes, since lighter nuclei have roughly the same number of protons and neutrons due to the charge-independence in the strong force acting to keep the nucleus together. However, as the nucleon number increases, the stable systems have more neutrons than protons because of the Coulomb-repulsion acting to separate the charged protons. Therefore the proton-rich side of the line of stability is extensively studied, whilst the neutron-rich nuclei still remain relatively unexplored. So far, the structure of some 4000 isotopes have been examined. More recently efforts are being made to reach the neutron rich side of the valley of stability via radioactive (neutron-rich) beams. Facilities for such experiments are currently under development at various laboratories. For instance, a large accelerator complex called FAIR (Facility for Antiproton and Ion Research) is planned at the present GSI site in Germany. This accelerator will be able to produce intense radioactive heavy ion beams up to energies of the order of tens of GeV per nucleon.

This thesis deals with studies of collective excitations and different types of nuclear deformation. Excited states in the isotopes of particular interest here (^{165}Lu and ^{107}Cd) are populated via heavy-ion fusion-evaporation reactions. The detected gamma rays following the de-excitations of these short-lived nuclei can be used to draw conclusions on their internal structure. However, knowing the energies of the excited states is not always enough for deducing the properties of the nuclei of interest. For instance, there has been many attempts to identify for deformed nuclei deviating from axially symmetrical shapes based on their intrinsic energy spectra, but there is still no firm experimental evidence for any such nucleus. Also vibrational and rotational modes of excitation are usually differentiated simply by analysing the energy spacing of excited states. Additional important information on the nuclear structure can be deduced by measuring the lifetimes of the excited states. Since the charge distribution within the nucleus is related to its shape, the shape affects the transition probability between excited states due to nuclear collective motion. The collective excitation mode of the nucleus affects the evolution of the transition probability as a function of increased angular momentum. A well deformed nucleus will rotate and the transition probability will approach a constant value at high angular momentum, whilst a vibrating nucleus will have an increasing transition probability as the angular momentum increases. Therefore, the lifetime of an excited state (which is inverse proportional to the transition probability) will give useful information on its shape and by analysing the evolution of the transition probability as a function of angular momentum, the excitation mode can be determined. The lifetime of a typical medium-spin nuclear energy level is of the order $\approx 1-100\times10^{-12}$ s. It is therefore clear that very precise techniques are needed to measure such short lifetimes. In this work the Recoil Distance Method is applied, in which the relation between the Doppler-shifted γ rays emitted from energy states decaying whilst the recoil is in flight, and the unshifted γ rays emitted after the recoil has come to rest in a stopper foil is analysed. Attempts have also been made to measure lifetimes of excited levels using the Doppler Shift Attenuation Method, with a thick target in order to stop the fusion products entirely. The ability to

resolve the energies of Doppler-shifted γ rays from the energies of unshifted γ rays is of high importance and would not be possible without high-resolution germanium detectors placed at different angles relative to the beam.

Chapter 2

Theoretical overview

Many theories have been developed to describe various aspects of the nuclear many-body problem. The base on which all of these theories rely, is that the nucleons are held together by the short-range attractive strong nuclear force, counteracting the repulsive Coulomb force, acting to separate the protons. Two different approaches used to explain the structure of nuclei are the nuclear shell model [1, 2], which works well for nuclei near closed shells, and the collective models [3, 4] taking a macroscopic perspective, which are more applicable to mid-shell nuclei. In the shell model the individual nucleons and single-particle excitations can be used to describe the energy levels and the structure of the entire nucleus. In the collective model the observed rotations and vibrations of the nucleus as a whole can be well described and used to explain the energy levels. For heavier nuclei it is often useful to consider a combination of the two different approaches, which assumes one or more valence particle(s) coupled to a collective core. There exists several different such methods combining the collective macroscopic properties of the nucleus with the microscopic shell effects for describing the shape of the nucleus as well as its energy levels. Another approach is the Interacting Boson Approximation (IBA) introduced by Arima and Iachello in 1974 [5]. The IBA model has proved useful when describing the excitation levels observed in nuclei in transitional regions between spherical vibrating nuclei and deformed rotating nuclei. Depending on its angular momentum or the number of valence nucleons, a nucleus can assume different shapes such as spherical or axially symmetrical deformed shapes. It is also possible for a nucleus to assume an axially asymmetric shape, i.e. a triaxial deformation.

2.1 The Nuclear Shell Model

This model is similar to the shell model for the electrons in the atomic shells. Using a simple potential like the isotropic harmonic oscillator together with the strong-interaction related spin-orbit coupling, the observed shell gaps with large binding energy for the so called “magic” nucleon numbers of 2, 8, 20, 28, 50,... are

reproduced. This inclusion of the $\ell \bullet s$ coupling for explaining the closed shells gave the Nobel Prize in physics 1963 to Maria Goeppert-Mayer and J. Hans D. Jensen. The obtained spherical shells are usually labeled by their orbital angular momentum and their total spin-orbit coupled angular momentum, $i = \ell + s$. The angular momentum of the orbit follow the same notation as in atomic physics, i.e. $s = 0, p = 1, d = 2, ...$ The actual nuclear potential is somewhere in between the harmonic oscillator potential and a square well potential. The often used Woods-Saxon potential satisfies the requirements on a realistic nuclear potential. It is more flat at the bottom and the edge is not as sharp as in the case of a square well. The disadvantage of using a Woods-Saxon potential is that the Schrödinger equation cannot be solved analytically. In all known nuclei with an even number of protons as well as an even number of neutrons, the ground-state has angular momentum 0, meaning that all nucleons couple two and two with opposite spin. Within the nuclear shell model an observed excited energy level in a spherical nucleus with an odd nucleon number can originate from a single particle excitation, i.e. the valence particle is excited into a different orbit. Another way to create excited energy levels in both odd nuclei and nuclei with an even number of protons and neutrons, is to break an opposite-spin coupled pair. It is then possible for these two new valence particles to get excited into different orbits. However, near the "magic" nucleon numbers the energy spacing is relatively large (in the order of one MeV). Excited states which are lower in energy can be produced if the nucleons from a broken pair couple to each other. The energy of the first excited state will then correspond to the pairing energy. The two freed nucleons are now able to couple to one another and if they occupy the same shell, even angular momentum values are produced. No odd values will be possible, since the antisymmetrised wave function only allows even values of the total angular momentum [6].

2.1.1 Deformed Shell Model (Nilsson model)

In order to better understand the underlying structure of deformed nuclear shapes we need to be able to calculate the energy levels for non-spherical shapes. The Nilsson model (which has its name after Sven Gösta Nilsson, who developed the theory in 1955 whilst working at the department of theoretical nuclear physics in Lund) or Modified Oscillator Model starts from the mathematically convenient harmonic oscillator potential. This harmonic oscillator potential is then allowed to be anisotropic, i.e. we let the potential along one of the axes, e.g. the nuclear z-axis, to be different from the extension along the x- and the y-axis, we may write the single-particle Hamiltonian in the following way [7]

$$H = -\frac{\hbar^2}{2M}\left(\frac{\partial^2}{\partial x^2} + \frac{\partial^2}{\partial y^2} + \frac{\partial^2}{\partial z^2}\right) + \frac{M}{2}\left[\omega_\perp^2 (x^2 + y^2) + \omega_z^2 z^2\right] - C\ell \cdot s \qquad (2.1)$$
$$-D(\ell^2 - < \ell^2 >_N)$$

The first two terms correspond to the anisotropic harmonic oscillator, the third

term is the spin-orbit term, giving rise to the splitting of the different ℓ, s states. The ℓ^2 term has the effect of interpolating between the square well potential and the harmonic oscillator potential. The parameters $C = 2\kappa\hbar\omega_0$ and $D = \mu\kappa\hbar\omega_0$ are parameters containing the oscillator frequency in the spherical potential and the two strength parameters κ and μ, different for the different major quantum number N-shells, are obtained from fits to experimental data. The anisotropy is achieved by the difference in $\omega_\perp$ and ω_z. To obtain this difference Nilsson introduced an elongation parameter $\epsilon = (\omega_\perp - \omega_z)/\omega_0$:

$$\omega_\perp = \omega_0(\epsilon)(1 + \tfrac{1}{3}\epsilon) \tag{2.2}$$
$$\omega_z = \omega_0(\epsilon)(1 - \tfrac{2}{3}\epsilon) \tag{2.3}$$

Negative values of ϵ correspond to a contraction along one of the nucleus main axes, i.e. an oblate shape. A positive ϵ corresponds to a contraction along two of the main axes and is called a prolate shape. Allowing for a deformed shape of the nucleus gives a splitting of the energy levels due to the different angular momentum projections of the valence particle on the symmetry axis of the nucleus (this quantum number is called K). For a prolate shape one can realise that levels with lower K (which means that the single-particle has its orbital angular momentum, ℓ, in the same direction as the nuclear angular momentum) comes lower in energy. For an oblate shape the opposite is true. The different energy splitted orbitals due to deformation can be labeled by the set of quantum numbers resulting from the symmetries of the nucleus

$$\Omega^\pi[Nn_z\Lambda] \tag{2.4}$$

where Ω is the projection of the single-particle angular momentum onto the symmetry axis, π is the parity quantum number described in section 2.1.2, N is the major quantum number, n_z is the number of oscillator quanta along the symmetry axis and Λ is the projection of the orbital angular momentum on the symmetry axis.

2.1.2 Cranked Shell Model

The main feature of the Cranked Shell Model (CSM), introduced by Inglis [8] and further developed by Bengtsson and Frauendorf [9], is that it treats the microscopic single particle excitations and the collective rotational excitations on the same footing. This is achieved by introducing the cranking Hamiltonian for a single particle, and by adding up the single particle Hamiltonians, one obtains the Hamiltonian for the nucleus as a whole. It is possible to derive a tilted axis cranking Hamiltonian [10] where the axis of rotation is not along one of the nucleus' main axes. However, a more simple approach to derive the cranking Hamiltonian is to introduce the rotation vector along one of the nucleus' main axes. The idea of a single particle moving independently in a rotating potential is described in a mathematical way by introducing the laboratory coordinates x, y z, and the coordinates in

the rotating system x', y', z'. For a constant angular velocity, ω, around the x'-axis we then get

$$x' = x \tag{2.5}$$
$$y' = y\cos\omega t + z\sin\omega t \tag{2.6}$$
$$z' = -y\sin\omega t + z\cos\omega t \tag{2.7}$$

Using the fact that the time-dependent wave functions and their derivatives with respect to time in the two coordinate systems must be the same, it can be shown that the following expression for the Hamiltonian in the rotating system is true,

$$h^{\omega} = h - \hbar\omega i_{x'} \tag{2.8}$$

where $i_{x'}$ is the intrinsic angular momentum projection on the rotational axis. Summing over all of the independent particle Hamiltonians gives,

$$H^{\omega} = H - \hbar\omega I_{x'} \tag{2.9}$$

The second term expresses the centrifugal and Coriolis term, which is due to the non-inertial coordinate system of the cranking Hamiltonian. The Coriolis force is acting to align the orbital angular momentum of the nucleons along the rotational axis of the nucleus. The energy eigenvalues of equation 2.9 are referred to as Routhians and not single-particle energies, since they are not the same as the single-particle energies observed in the laboratory frame of reference. Hence, the disadvantage of using the cranking model is that the wave functions are not eigenstates of the angular momentum operator any longer. It can be shown that for a harmonic oscillator potential, the moment of inertia using the CSM is the same as the static moment of inertia for a rigid rotor.

Parity and Signature

In the axially symmetric case, the only two quantum numbers still conserved under rotation are the parity, π, and the signature, α. The parity quantum number is $\pi = +1$, if the wave function is still positive after inversion of all spatial coordinates ($\mathbf{r} \rightarrow$ **-r**) or $\pi = -1$, if the wave function changes sign after the inversion. The signature quantum number is defined by

$$I = \alpha\,(mod2) \tag{2.10}$$

and describes the invariance with respect to a rotation of 180° around the rotational axis. For an even-mass nucleus α is 0 or 1 and for odd-mass nuclei it takes the values $\pm\frac{1}{2}$.

2.2 The Liquid Drop Model

An early version of the phenomenological Liquid Drop Model (LDM) was first proposed by George Gamow [11] in the late 1920's. The LDM describes the nucleus as an incompressible fluid and was suggested in order to explain the different properties of the nucleus, such as mass and binding energy. Using this model for explaining the energy levels of the nucleus works best for spherical mid-shell nuclei, which experiences collective phenomena in terms of vibrations of the nuclear core. An important feature of the quantum liquid drop is that the velocity distribution does not have to be isotropic, which is the case in a normal droplet. Again, this is due to the fact that the mean-free path inside the nucleus is long, such that scattering events are considered negligible.

2.2.1 Deformed Liquid Drop

In the early 50's Aage Bohr, Ben Mottelson and Leo Rainwater [12, 13, 14] managed to describe the collective excitations in nuclei in terms of rotations and vibrations of its core. They also worked out the connection between these collective excitations and the shell-model based single-particle excitations. For this work they were awarded the Nobel prize in 1975.

Since the wave-function can not distinguish between different angular orientations for a spherical object, we have to introduce some deformation parameters to allow for anisotropy in the distribution of the density to achieve a gain in energy. This means that we will allow for surface oscillations of a spherical or deformed shape and in the deformed case, also rotations around an axis perpendicular to the symmetry axis would lead to an increase in energy. The length of the radius vector pointing from the center to a point on the "surface" (note that the surface of the nucleus is not well defined and is usually approximated to the place where the nuclear matter density assumes half its central value) can be described by performing the expansion in the spherical harmonics, $Y_{\lambda\mu}$ [15],

$$R(\theta,\phi) = R_{av}\big(1 + \alpha_{00} + \sum_{\lambda=1}^{\infty}\sum_{\mu=-\lambda}^{\lambda} \alpha^{\star}_{\lambda\mu} Y_{\lambda\mu}(\theta,\phi)\big) \tag{2.11}$$

where R_{av} is the radius of a sphere with the same volume. The constant α_{00} is chosen such that the volume of the nucleus is the same at all deformations and λ is the multipole order of the shape. It can be shown that $\lambda = 1$, i.e. dipole deformation, corresponds to a displacement of the center of mass and can therefore not result from internal nuclear forces. Considering an axially symmetric deformed object with the z-axis as the symmetry axis, gives the result that $\alpha_{\lambda\mu}$ vanishes except when $\mu = 0$. These deformation parameters $\alpha_{\lambda 0}$ are usually called β_λ, [16]. The relation between the different parametrisations of the nuclear deformation, ϵ, introduced in the Nilsson model and β are, in general, non-trivial. However, for

the axially symmetric case the relationship between the quadrupole deformation parameters (ignoring multipoles of higher order), ϵ_2 and β_2 is [17]

$$\beta_2 = \sqrt{\tfrac{\pi}{5}}(\tfrac{4}{3}\epsilon_2 + \tfrac{10}{63}\epsilon_2^2 + \tfrac{2896}{6615}\epsilon_2^3 + \ldots) \tag{2.12}$$

$$\epsilon_2 = \tfrac{3}{4}\sqrt{\tfrac{5}{\pi}}\beta_2 - \tfrac{75}{224\pi}\beta_2^2 - \tfrac{81}{128\pi}\sqrt{\tfrac{5}{\pi}}\beta_2^3 + \ldots \tag{2.13}$$

The shape can of course also be parametrised in an axially asymmetric way. In the case of a quadrupole deformation ($\lambda = 2$), μ can assume five different values and we end up with five parameters $\alpha_{2\mu}$. Only two of these describe the shape of the drop, the other three determine the orientation of the drop in space. If we choose the body-fixed system to coincide with our coordinate system, the shape of the nucleus can be specified by the β parameter, as mentioned above, and the triaxial deformation parameter γ. They are related to the non-vanishing $\alpha_{2\mu}$ coefficients in the following way

$$\alpha_{20} = \beta_2 \cos\gamma, \quad \alpha_{22} = \tfrac{1}{\sqrt{2}}\beta_2 \sin\gamma \tag{2.14}$$

It is now possible to derive the nuclear surface for an axially asymmetric quadrupole shape by evaluating the spherical harmonics in eq. 2.11, which gives the result

$$R(\theta,\phi) = R_{av}\left[1 + \beta_2\sqrt{\frac{5}{16\pi}}(\cos\gamma(3\cos^2\theta - 1) + \sqrt{3}\sin\gamma\sin^2\theta\cos 2\phi)\right] \tag{2.15}$$

See fig. 2.1 for the different quadrupole deformed nuclear shapes. One way to visualise a triaxial deformation is to consider a prolate (axially symmetric) deformed object. If this object is squeezed in a direction perpendicular to the symmetry axis, the former prolate shape will transform into an axially asymmetric shape. A cross section across the former prolate symmetry axis of such a body would no longer be circular, instead an ellipsoid cross section is observed.

2.3 The Strutinsky Shell Correction Method

The liquid drop model describes very well vibrations of nuclei with nucleon numbers in between shell gaps where the shell effects are negligible. However, the minimum energy using this model is always obtained by a spherical shape. Many examples of nuclei with deformed ground states are existing in nature and the LDM model also fails to reproduce the energy levels as the nucleon numbers approach closed shells. Strutinsky therefore introduced his method in 1967 [18] of adding a deformation dependent shell correction term to the liquid drop energy, $\delta E_{sh}(def)$. The bulk properties are taken care of by the liquid drop part of the energy and the microscopic quantal effect of the shell gaps are taken care of by the shell correction term. The total energy of the nucleus thus becomes

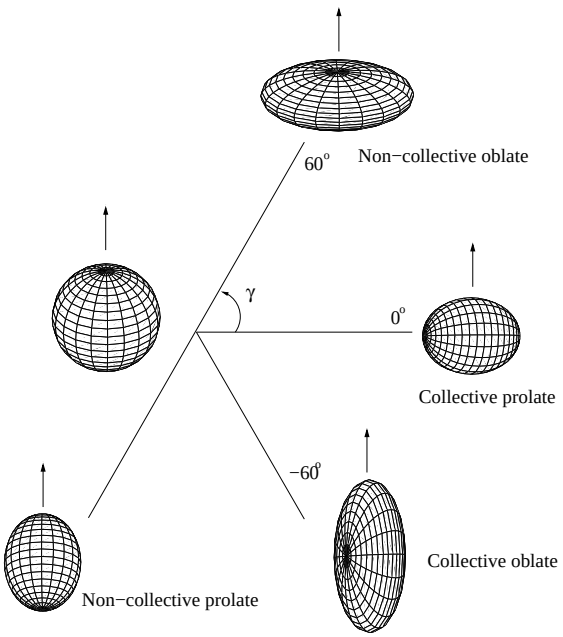

Figure 2.1: The different quadrupole deformations in the β_2, γ plane. The angles, $\gamma = 0°, 60°, -60°, -120°$, corresponds to a prolate collective, oblate non-collective, oblate collective and prolate non-collective rotation respectively.

$$E_{tot}(def) = E_{L.D.}(def) + \delta E_{sh}(def)(prot) + \delta E_{sh}(def)(neut) \tag{2.16}$$

for any set of deformation parameters (def). The shell model part can be large enough to produce energy minima at high angular momentum for deformations with the axis ratio 2:1, so called superdeformations.

2.4 Vibration

It is sometimes possible to describe observed nuclear excitation spectra in terms of surface oscillations, or vibrations, about a spherical or a deformed shape. The surface coordinates $\alpha_{\lambda\mu}$ $(\lambda \geq 2)$ are considered to be functions of time. Small fluctuations about a spherical equilibrium can then be described by the Hamiltonian of a harmonic oscillator form

$$H = T + V = \frac{1}{2}\sum_{\lambda\mu}\{B_\lambda|\dot{\alpha}_{\lambda\mu}|^2 + C_\lambda|\alpha_{\lambda\mu}|^2\} \tag{2.17}$$

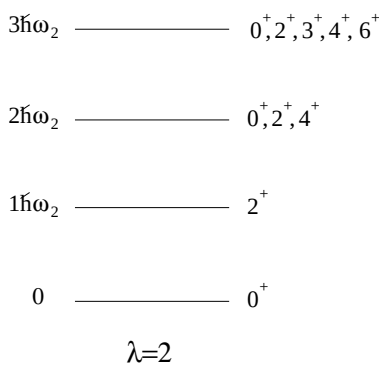

Figure 2.2: Energy spacing of quadrupole phonon excitations of a spheroid.

where B_λ and C_λ are the collective mass and stiffness parameter, respectively. Performing a second quantization, with the creation and annihilation operators $b^\dagger_{\lambda\mu}, b_{\lambda\mu}$ acting to create or annihilate *phonons* [19], provides the following Hamiltonian

$$H = \sum_{\lambda\mu} \hbar\Omega_\lambda (b^\dagger_{\lambda\mu} b_{\lambda\mu} + \frac{1}{2}) \tag{2.18}$$

with the frequencies $\Omega_\lambda = \sqrt{C_\lambda / B_\lambda}$. It then follows that for each λ we have a harmonic spectrum of surface vibrations, such a spectrum can be seen in fig. 2.2 for the quadrupole ($\lambda = 2$) case. For quadrupole shapes, it turns out that for $\mu = 0$ the axial symmetry is preserved and they are referred to as β vibrations, for $\mu = \pm 2$ (γ vibrations) the axial symmetry is broken.

The reduced matrix element for a transition between states of spin difference $I_i - I_f = 2\hbar$, between the different phonon excitations for a vibrator of quadrupole type are proportional to the square root of the phonon number, $\sqrt{N_{ph}}$. Hence, the reduced transition probability, $B(E2)$, described further in sect. 2.5.1, is proportional to N_{ph}. This can be shown by considering the decay probability of a one-phonon state to the ground state to be unity. Since multi-phonon excitations simply consist of piling of more than one identical phonon, it might seem like the value of the $B(E2)$ of a two-phonon decay would also be unity. However, the initial state has two phonons and either one of them can be destroyed, therefore we have twice as many decay possibilities and $B(E2 : N_{ph} = 2 \rightarrow N_{ph} = 1) = 2$. Following the same procedure for increasing phonon number gives the relation, $B(E2) \propto N_{ph}$.

2.5 Rotation

The most striking feature resulting from allowing the nucleus to assume a permanent deviation from sphericity is the possibility for the nucleus to gain energy

by a rotation around an axis perpendicular to the symmetry axis, since the wave-function now has a ϕ dependence. The energy levels can be approximated from the kinetic energy of a rigid rotor, which classically can be described by $E = \frac{1}{2}\jmath\omega^2$, where $\jmath$ is the moment of inertia. Replacing $\jmath\omega$ with the angular momentum ℓ, and using the fact that for a quantum object we have, $\ell^2 = \hbar I(I+1)$, where I is the angular momentum quantum number, we arrive at the following equation for the energy levels

$$E = \frac{\hbar^2}{2\jmath} I(I+1) \tag{2.19}$$

As mentioned in the introduction to the chapter on the nuclear shell model; within a nucleus in its ground state having an even number of protons and neutrons, like nucleons always couple into pairs moving in time-reversed orbits. That implies identical orbits with the velocity vectors in opposite directions, meaning that the different intrinsic angular momenta, i, always cancel and the ground state of all even-even nuclei has $I^\pi = 0^+$. The rotational band for even-even nuclei can contain only even *or* only odd values of I, since the axially symmetric deformed shape is invariant with respect to a rotation of 180° around the rotational axis. Equation 2.19 gives the typical value of 3.33 for the ratio $E(4^+)/E(2^+)$.

In the case of odd nuclei a particle-plus-rotor model, where the bulk properties of the nucleons undergoes a rotation and the effects of the nucleon(s) outside a closed shell are added to the core, proves useful. The rotational alignment of the valence nucleon, i_x, and its projection on the symmetry axis, K, for a prolate nucleus is illustrated in fig. 2.3.

In the strong coupling scheme, the rotational spectra starts at the single-particle spin-projection on the symmetry axis, K. The single-particle orbital typically has a large K value, i.e. the nucleon orbits in a plane perpendicular or nearly perpendicular to the rotational plane of the core. As the nucleus increases its rotational frequency, the Coriolis force ($\propto \omega \times \mathbf{v}$) will act to align the valence nucleon along the rotational axis. If we have two valence nucleons moving in time-reversed orbits, the Coriolis force will act to break up the pair and align the particles along the rotational axis. When this occurs there will be a decrease in the energy level spacing and an increase in angular momentum. This phenomenon is referred to as back-bending, since a plot of the moment of inertia as a function of the rotational frequency will show a back-bending curve.

If the angular momentum vector of the valence nucleon is instead aligned along the rotational axis (low values for K), we expect the Coriolis force to be strong and the band head is not necessarily the same as the K quantum number, since the energy states of higher angular momenta can be lower in energy than the state with angular momentum K. For $K \neq 0$, all spin values $\geq K$ are allowed and the two possible energy sequences of I makes it convenient to divide the band into its two signature (introduced in eq. 2.10) partners, each with the spin difference $2\hbar$. The two rotational bands with different signatures are built on the two time-reversed

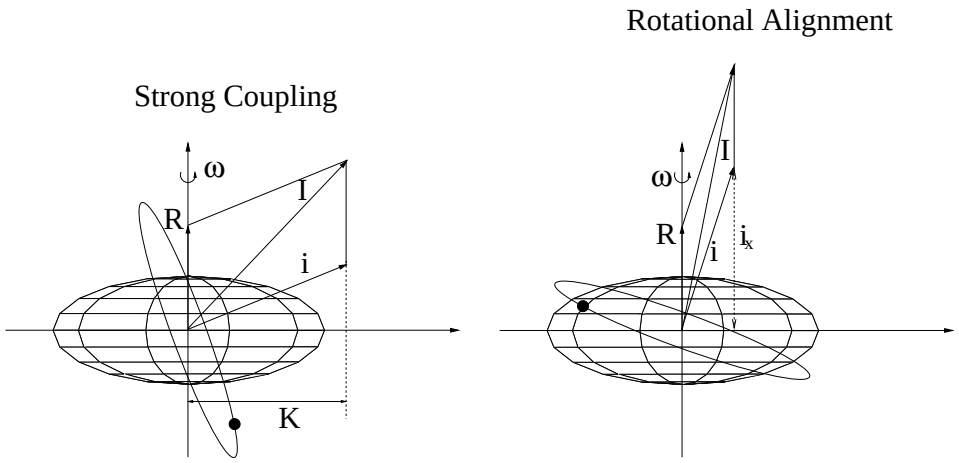

Figure 2.3: Illustration of the strong coupling and rotational alignment of the valence nucleon to a prolate deformed core. The projection of the valence nucleon angular momentum on the rotational axis, i_x, and the symmetry axis, K, are visualised.

orbitals. In the rotational spectra, the difference between bands built on a low-K orbital (with large angular momentum, i) and bands built on a high-K orbital is visible in the different energy splittings between the signature partners. For large values of K the Coriolis force is weak and there will be little energy difference between the different signature bands. The band starting at spin $K + 1$ will be connected to the band starting at spin K via $\Delta I = 1\hbar$ γ-ray transitions of equal, or close to equal, decaying and feeding γ-ray energies. The energy levels of the band starting at $K+1$ will thus be placed in the middle between two energy levels of the rotational band with the band head of spin K. The Coriolis force is expected to be weak in this case since this force is proportional to $(\omega \times \mathbf{v})$ and when the orbit of the nucleon is perpendicular to the symmetry axis of the nucleus (i.e. a high-K band), the time averaged expectation value of the cross-product will be zero. On the other hand, for a low-K band the energy difference is expected to be high, since the cross-product is now large and depending on the direction of the velocity vector the force is pointing in different directions. In many cases the band starting at $K+1$ is too high in energy in relation to its low angular momentum, (i.e. it is too far away from the so called *yrast* line connecting the states with the lowest energy for the highest angular momentum, see sect. 3.1) to be seen in the energy spectra of a nucleus created in a fusion-evaporation reaction. However, high-K bands can also show a signature splitting due to mixing of wave-functions with different K values, one way to achieve such "K-mixing" is to allow for a triaxial deformation

of the nucleus.

2.5.1 Quadrupole Moment

Another consequence following the anisotropic matter distribution inside the nucleus is the intrinsic quadrupole moment, which can be written for a rotating axially symmetric deformed shape as [17]

$$Q_0 = \frac{3}{\sqrt{5\pi}} R_{av}^2 Z\beta_2(1 + \frac{1}{8}\sqrt{\frac{5}{\pi}}\beta_2 + \ldots) \tag{2.20}$$

where Z is the proton number and $R_{av} = R_0 A^{1/3}$, A is representing the nucleon number and R_0 is 1.2 fm. Assuming a rotational model gives the quadrupole moment related, via the Clebsch-Gordan coefficient for a transition from the state I to the state $I-2$, to the reduced transition probability in the following way

$$B(E2; I \rightarrow I-2) = \frac{5}{16\pi} Q_0^2 | < IK20|I-2K > |^2 \tag{2.21}$$

The Clebsch-Gordan coefficient is given by

$$< IK20|I-2K >= \sqrt{\frac{3(I-K)(I-K-1)(I+K)(I+K-1)}{(2I-2)(2I-1)I(2I+1)}} \tag{2.22}$$

It can thus be seen that the $B(E2)$ value, assuming a rotational model approaches a constant value at high spins ($< IK20|I-2K > \approx \sqrt{3I^4/8I^4}$ for large values of I), as opposed to the vibrational model where it increases, see sect. 2.4. The quadrupole reduced transition probability can also be deduced from the lifetime, τ, of an excited nuclear state in a model-independent way (see also section 3.1.1)

$$B(E2; I \rightarrow I-2) = \frac{1}{\tau} \frac{1}{1.223 \times 10^9 E_\gamma^5} \tag{2.23}$$

where E_γ is the energy difference between the I and the $I-2$ state. From the above discussion it follows that the transition probability, and thereby the lifetime of an excited state, is linked to the deformation of the nucleus, in a model-dependent way as discussed in **paper I**. The quadrupole moment for an axially asymmetric nucleus can also be deduced and equation 2.20 then changes to

$$Q_0 = \frac{6}{\sqrt{15\pi}} R_{av}^2 Z\beta_2(1 + \frac{1}{8}\sqrt{\frac{5}{\pi}}\beta_2 + \ldots) \times (\cos(\gamma + 30^\circ)) \tag{2.24}$$

The reduced transition probability deduced from the quadrupole moment also has to be corrected for the triaxial asymmetry [20]. One thus obtains

$$B(E2; I \rightarrow I-2) = \frac{5}{8\pi} Q_0^2 \frac{(I-1)I}{(2I-1)(2I+1)} \times \left[\cos(\gamma + 30^\circ) - \cos(\gamma - 30^\circ)\frac{K^2}{(I-1)I}\right]^2 \tag{2.25}$$

2.6 Interacting Boson Approximation

We have now looked at different collective models for explaining the observed energy levels within atomic nuclei, the vibrational and the rotational model. Another way that has proved successful in describing the collective excitations of the nuclear system is the so called Interacting Boson Approximation introduced in 1974 by Arima and Iachello [5]. This model is a group-theory based algebraic model. The bulk properties of the nuclear core are added to a certain number of valence bosons outside a closed shell. The assumption is that all of the valence fermions couple to bosons of angular momentum 0 or 2, called s or d bosons. The increase in angular momentum and energy is due to interactions between these bosons. The d bosons ($I = 2$) have five magnetic sub states and the s bosons ($I = 0$) have one, so the basis states of this $s - d$ boson system span a six-dimensional space. It turns out that such a system can be described within the U(6) algebraic group. This group can then be divided into different subgroups, one of which is the U(5) vibrational limit. The eigenvalues of the U(5) limit are not functions of the number of s bosons, only the number of d bosons, n_d, contribute to the energy levels. The collective excitations can then be described by the interaction of such d boson pairs. The reduced transition probability in the U(5) limit is given by [21]

$$\sum_{I_f} B(E2 : I_i, n_d \rightarrow I_f, n_d - 1) = n_d(N - n_d + 1)e_B^2 \tag{2.26}$$

If the angular momentum selection rules (see section 3.1.1) allow decay to more than one level of the next lower multiplet, the different distribution strengths are taken into account by the sum over all final angular momenta. N is the total number of valence bosons, I_i is the spin of the initial level and e_B^2 is a boson charge similar to the effective charge for fermions. For successive yrast states with $\Delta I = 2$, which decays via stretched (i.e. the angular momentum of the transition is equal to the spin difference of the involved levels) quadrupole transitions to an yrast state of spin $I_f = I_i - 2$ of the same parity as the initial state, the number of d bosons , n_d, is equal to $I_i/2$. The reduced transition probability can then be rewritten as

$$\begin{aligned} B(E2 : I_i, n_d \rightarrow I_f, n_d - 1) &= B(E2 : \frac{I_i}{2} \rightarrow \frac{I_i}{2} - 1) && (2.27) \\ &= \frac{I_i}{2}(N - \frac{I_i}{2} + 1)e_B^2 && (2.28) \end{aligned}$$

If the spins corresponding to the different d bosons are considered, i.e. $I = 0, 2, 4, 6, \ldots$, It then holds that for transitions between successive yrast states, the ratio of the reduced transition probability for a transition from a state of spin I to $I - 2$ and the reduced transition probability to the ground state is

$$\frac{B(E2 : I \rightarrow I - 2)}{B(E2 : 2^+ \rightarrow 0^+)} = \frac{1}{4}\frac{(I)(2N - I + 2)}{N} \tag{2.29}$$

A consequence of this formula is that n_d can only vary between 0 and N. The transition rate is zero if n_d is larger than N.

It has thus been shown from the previous sections that the $\frac{B(E2:I\rightarrow I-2)}{B(E2:2^+\rightarrow 0^+)}$ ratios can be used as a probe for the excitation mode of the nucleus, since the ratios are different depending on the type of excitation.

2.6.1 $B(E2)$-plots

Important information regarding the mode of excitation can be extracted from the evolution of the reduced quadrupole transition probabilities as a function of angular momentum [22]. The $B(E2)$ value for an ideal harmonic vibrator is proportional to the phonon number, $n = \frac{I}{2}$, of the initial state for an yrast transition with spin difference $\Delta I = 2$. However, for an axially symmetric rotor the ratio of the transition probabilities of the state of interest and that of the first excited state is simply the square of the ratio of the Clebsch-Gordan coefficients, see eq. 2.21. This ratio first increases and at higher spins it tends towards a constant value. In the U(5) vibration limit the ratio first increases slightly and then decreases until it reaches the value of one when the spin is equal to the maximum possible spin by coupling of the valence bosons. By plotting the $B(E2)$ ratios as a function of spin and examining the slope, the excitation mode can be determined. An example of such a plot can be seen in fig. 2.4. In this way it will also be possible to discover a transition from a vibrational excitation mode to a rotational behaviour as discussed in **paper II**.

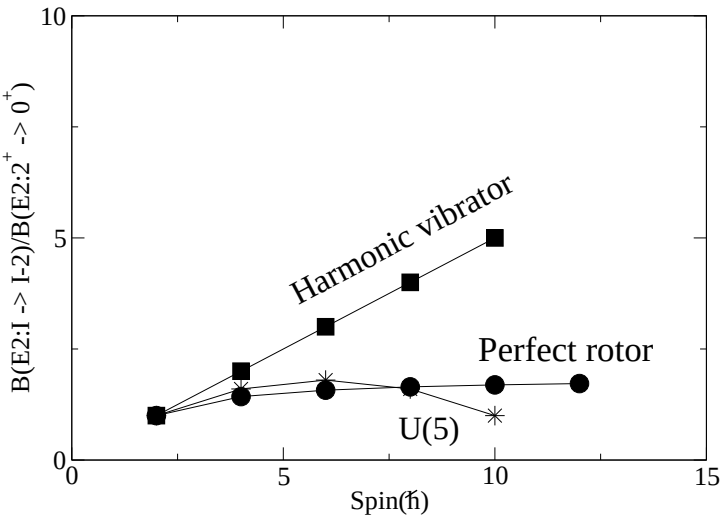

Figure 2.4: The ratio of the $B(E2 : I \rightarrow I-2)$ for the state of interest and the $B(E2)$ for the transition to the ground-state, as a function of spin. The ratios for a harmonic vibrator (see section 2.4), perfect rotor (see section 2.5) and the U(5) limit (according to eq. 2.29 with five valence bosons) are marked with squares, circles and stars respectively.

Chapter 3

Experimental Techniques and Data Analysis

As previously discussed, it is possible for the nucleus to assume different shapes, such as spherical and deformed axially symmetric shapes. Also axially asymmetric shapes; triaxial shapes, are theoretically possible, although it has proved to be difficult to find unique experimental probes for these shapes. One commonly used indicator of triaxiality is the signature splitting of strongly coupled rotational bands where the triaxiality would allow for states with different K-values to mix into the wave function. However, signature splitting and K-mixing could also occur in strongly coupled bands in axially symmetric nuclei when the rotation alignment of the valence particle increases with increasing spin due to the Coriolis interaction, see section 2.5. Another way to probe triaxiality is to measure the lifetimes of the excited levels, deduce the transition probabilities and using a collective rotational model to deduce the quadrupole moments, which are related to the charge distribution and the shape of the nucleus. It has also been shown in the previous chapter that the evolution of the transition probability as a function of spin is different for a vibrator and a rotor. This shows that information on the lifetime can give useful information regarding the excitation mode of the nucleus. Therefore, experiments to measure the transition probability of the excited levels in the nucleus are important. There exists different experimental methods to obtain the $B(E2)$ values, such as Coulomb excitation, inelastic electron scattering or by measuring the lifetimes of the excited states. For high spins the best method is to measure the lifetimes of the excited levels created in fusion-evaporation reactions from heavy-ion collisions. Several different ways of measuring the lifetimes are existing and the chosen method depends on the expected lifetime.

3.1 Compound Nucleus Formation

Via the collision of heavy ions a residual nucleus in a state of high angular momentum and excitation energy can be formed. Since the collisions, described within this thesis, involve two lighter stable ions the resulting nucleus will be on the neutron deficient side of the valley of stability. As mentioned in the introduction, lighter stable nuclei have the same number of protons and neutrons since the strong force is independent of nucleon-type. As the proton number increases, the Coulomb force becomes relatively more important and the line of stability bends towards isotopes with a larger number of neutrons than protons. It is therefore possible to study nuclei close to the proton drip-line using fusion-evaporation reactions with stable ions. To reach the neutron-rich side, radioactive beams (or targets) have to be used and these techniques are currently under development or explored at different laboratories, for example at GSI [23] and GANIL [24] in Europe, at RIKEN [25] in Japan and at ORNL [26], MSU [27] and TRIUMF [28] in North America. The most common types of accelerators used are of a cyclotron, linear accelerator, or a tandem-accelerator type. The experiments performed to populate high spin-states in the nuclei of particular interest in this thesis, i.e. ^{165}Lu and ^{107}Cd, took place at Laboratori Nazionali di Legnaro, Italy and at the Wright Nuclear Structure Laboratory at Yale University, USA respectively. Both laboratories are using tandem accelerators to create the beam. The bombarded heavier ion target-foil with a high purity in isotope species is in a fixed position. In such a heavy-ion collision a compound nucleus may be formed. This intermediate stage has a short lifetime of the order $\approx 10^{-18}$ s. The collided ions are completely fused together and the resulting compound nucleus is often considered to be in a hot state of thermal equilibrium. Therefore, the different ways of de-excitation of the compound system in a given state of energy and angular momentum are not depending on how it was created. An illustration of a fusion-evaporation reaction can be seen in fig. 3.1. The beam energy should be optimised for this type of reaction. If the energy is too low the beam will not exceed the Coulomb barrier and if the energy is too high, direct reactions and fragmentation will take place instead. An optimum energy for a fusion-evaporation reaction is $\approx 3 - 5$ MeV/A in the centre-of-mass system, depending on the beam-target combination. The beam energy has to be chosen more carefully in order to achieve the desired reaction channel, i.e. the correct number and type of evaporated particles, with optimal cross-section. When the excitation energy of the residual nucleus is too low to allow for further evaporation of particles it continues to de-excite by emitting photons. First, the nucleus will emit "statistical photons" of relatively high energy and low angular momentum from the continuum of energy states generally down close to the "line" connecting states with the lowest energy for a certain angular momentum. This line is referred to as the *yrast* line. When the yrast line is reached the nucleus normally continues to decay down this path until it reaches its ground-state. Experimentally it is difficult to populate states high above the yrast line in a fusion-evaporation reaction.

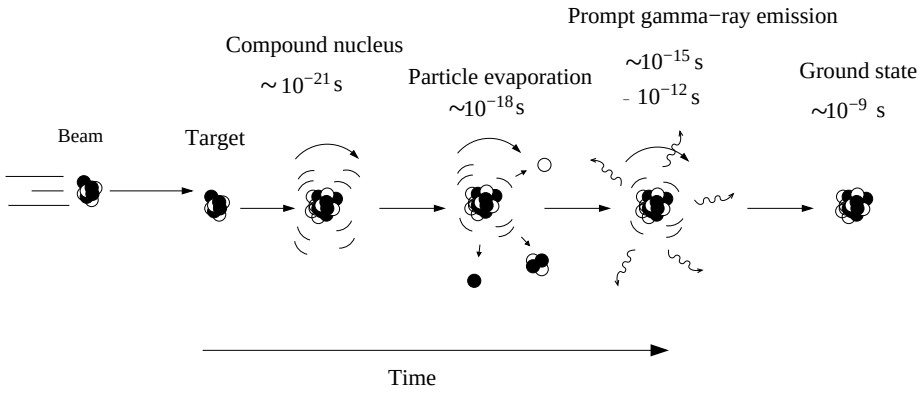

Figure 3.1: A schematic view of compound nucleus formation and its decay, following the collision of heavy ions.

3.1.1 Angular Distribution of Photons

The angular distribution of a γ decay can be described by the Legendre polynomials, $P_{2L}(\cos\theta)$, where L is the multipole order. The most common cases of γ radiation from excited nuclear states are dipole and quadrupole radiation, for which $P_2 = \frac{1}{2}(3\cos^2\theta - 1)$ and $P_4 = \frac{1}{8}(35\cos^4\theta - 30\cos^2\theta + 3)$ respectively. The selection rules for the angular momentum and parity of a transition from I_i to I_f are as follows [29]:

$$\begin{aligned} |I_i - I_f| \leq L \leq I_i + I_f \\ \Delta\pi = \text{ no: even electric (E), odd magnetic (M)} \\ \Delta\pi = \text{ yes: odd electric (E), even magnetic (M)} \end{aligned} \tag{3.1}$$

The exception is when $I_i = I_f = 0$, since there are no monopole transitions in which a single photon is emitted. The lowest possible multipole is always favoured, since the reduced transition probability decreases with increasing L according to

$$B(\lambda L : I_i \rightarrow I_f) = \frac{1}{\tau}\frac{\hbar L((2L+1)!!)^2}{8\pi(L+1)}\left(\frac{\hbar c}{E_\gamma}\right)^{2L+1} \tag{3.2}$$

where λ is either magnetic or electric, E_γ is the energy of the transition and τ is the lifetime of the state. However, a transition between states of the same parity and differing by one $\hbar$ in total angular momentum, does generally (depending on the energy difference between the two states) have a contribution from $\lambda L = E2$ transitions. Since the heavy-ion collision will polarize the radiation field of the recoils, the $M1/E2$ mixing ratio can be determined by analysing the intensity of the photons at different angles.

3.2 Ge Detectors

Surrounding the reaction point, large systems of germanium detectors are placed for detection of the emitted photons. When a photon interacts with an electron within the depletion region of the semiconductor crystal inside one of the detectors, the resulting energetic electron slows down via collisions onto several other electrons. These electrons are then excited from the valence band into the conduction band, leaving a hole in the valence band. The average energy needed for creating one such electron-hole pair is ≈ 3 eV. The electrons will then start to drift towards the anode and the holes towards the cathode. The induced current that the electrons and holes produce will be observed at the output of the detector. To create the active region, or the depletion region, a bias high voltage, V, has to be supplied since the thickness of the depletion region is given by [30]

$$d = \sqrt{\frac{2\epsilon V}{eN}} \tag{3.3}$$

where N is the net impurity concentration in the semiconductor material, ϵ is the dielectric constant and e is the electronic charge. To achieve a depletion gap of around 1 cm, a typical voltage for a high purity germanium (HPGe) detector is in the order of a couple of kV. To avoid thermal excitations across the band gap, which is only 0.7 eV, the detector is cooled with liquid nitrogen down to 77K.

There are three main types of possible interactions between the incoming photon and the atoms within the crystal when the γ ray hits the detector, namely Compton scattering, pair production, and photo absorption. In the analysis events containing the final photo absorption, where the entire energy of the photon is transformed to an electric pulse in the detector, are desired. Since the cross section for our reactions is generally very low, a large number of detectors covering large angles are needed to improve the efficiency for photon detection. Another feature of high importance resulting from the use of several detectors is the possibility to place the γ rays in relation to each other in an energy-level diagram, by requiring different coincidence relations of the photons. The SPEEDY Ge-detector array used in the experiment resulting in **paper II** is situated at the WNSL at Yale in the USA and it consists of eight Compton-suppressed clover detectors [31], placed in the two symmetric angles of 41.5^o and 138.5^o relative to the beam line. Each clover detector consists of four leaves, i.e. four segments of germanium crystals. In an array with segmented Ge detectors it is possible to improve the efficiency when the segments are used in so called add-back mode, i.e. the Compton scattered events are added back together to produce the full energy peak. However, in our experiment the high γ-ray fold reduced the isolated hit probability and therefore made the clovers more powerful in non add-back mode, essentially meaning that the eight clovers could be regarded as 32 separate detectors. The experiment resulting in **paper I** was performed at LNL in Italy and used the GASP Ge-array [32], consisting of 40 Compton-suppressed detectors at the eight symmetric angles of 34°, 60°, 72°, 90°, 108°, 120°, and 146° relative to the beam line, a picture of this array can be seen

in fig. 3.2. The detectors are surrounded by Bismuth-Germanate (BGO) detectors with a high detection efficiency for γ rays. If a pulse is recorded from one of the Ge-detectors and another pulse is recorded in the surrounding BGO detector in the same event, the photon is assumed to be Compton-scattered inside the Ge crystal and the information from this particular detector is removed from the event in the off-line analysis.

3.3 Data Analysis

The data from the fusion-evaporation events were saved and analysed off-line. The digitally converted information extracted from the electrical pulses from the semiconductor detectors consisted of the relative timing and the energies of the detected photons. After calibration and gain matching using a standard ^{152}Eu source, the energy spectra were obtained and analysed. Prompt gamma rays were chosen by selecting an appropriate coincidence window of ≈ 50 ns in the Ge timing spectra and the photon energies were then sorted into γ-γ coincidence matrices. Two or more detectors firing within a certain time-window produces a point in a $E_{\gamma_1} - E_{\gamma_2}$-matrix for each combination of the two photon energies. The matrix is then projected onto the two axes and it is now possible to deduce the coincidence information by choosing a slice around a certain transition energy within the nucleus of interest, and analyse the projection of this slice onto the other axis. In this way photons emitted in coincidence with one another can be analysed. One matrix was obtained for each unique combination of angles relative to the beam line. In the RDM analysis (see sec. 3.4.2) these matrices were also sorted for each target-stopper distance.

3.4 Measuring Lifetimes

The method used to obtain the lifetimes of excited states depends on the expected time range. For very short lifetimes, $\approx 10^{-12} - 10^{-15}$ s, e.g. relevant for collective high-spin states, the Doppler Shift Attenuation Method [33] (DSAM) is a powerful technique. For lower spin states, longer lifetimes in the order of 1-100 ps are expected. In this case the Recoil Distance Method [33] (RDM) can be used to deduce the lifetimes. The two experiments discussed in this thesis were both aimed to measure the lifetimes of excited nuclear states using the RDM technique. However, in the experiment resulting in **paper II** part of the beam time was devoted to a DSAM experiment. A thick target with gold backing was used in order to stop the fusion products entirely inside the target. It later showed that the statistics in this part of the experiment was too poor in order to perform a proper analysis on the most interesting states using this method and the results from the DSAM analysis have therefore not been published. Both the DSAM analysis and the RDM technique are described below. For even longer lifetimes of isomeric states within nuclei, it is possible to use direct electronic timing information, e.g. with the aid of

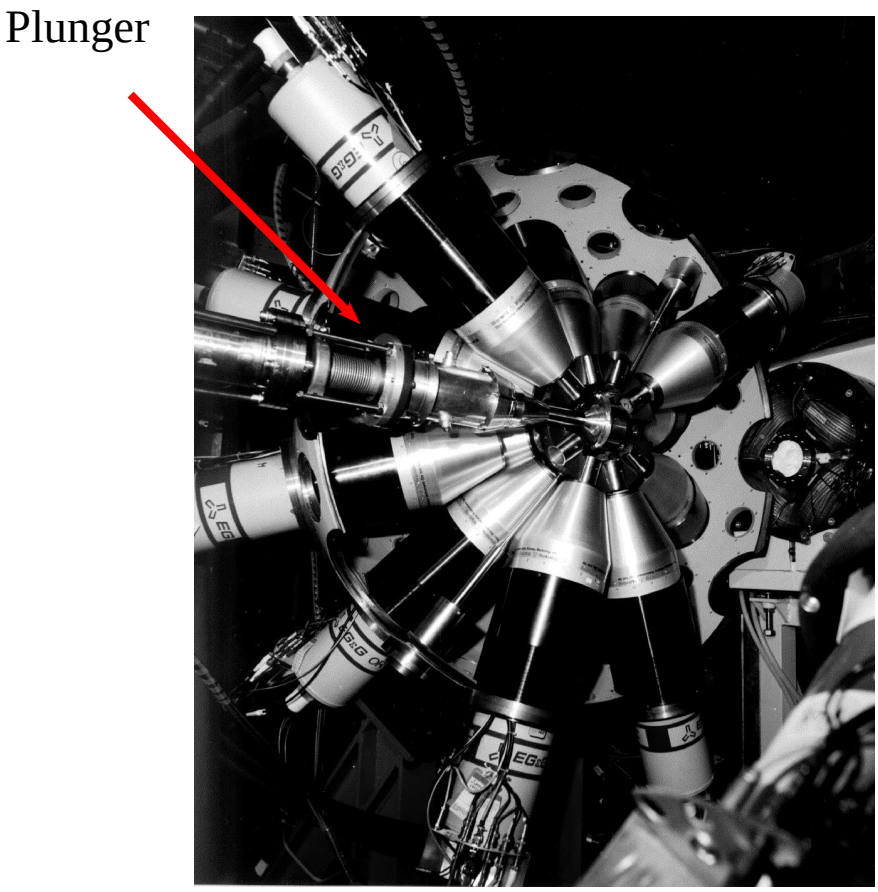

Figure 3.2: One half sphere of the Ge-array at Laboratori Nazionali di Legnaro, consisting of 40 Ge detectors, used together with the Cologne plunger, described in section 3.4.2.

techniques using mass separators and implantation of the recoils into silicon-strip detectors or pulsed beams.

3.4.1 Doppler Shift Attenuation Method

The idea behind the Doppler Shift Attenuation Method (DSAM) is to use a target with a thick backing of a heavy mass number (e.g. gold) to stop the recoils entirely. The average velocity of the recoils when emitting a certain γ ray can be deduced by analysing the centroid of the Doppler shifted energies. The shifted photon energies (evaluated in the laboratory frame of reference) is

$$E_{\gamma'} = E_{\gamma}\frac{\sqrt{1-\frac{v^2}{c^2}}}{1-\frac{v}{c}\cos\theta} \tag{3.4}$$

where $E_{\gamma'}$ and E_{γ} are the measured shifted and unshifted energies of the photon, respectively. The velocity of the recoils is denoted by v, c is the speed of light and θ is the angle between the direction of the beam and the detector. Using this equation and measuring the energy of the centroid of the total lineshape, the average velocity when the γ rays were emitted (v_{av}) can be determined. The attenuation factor as a function of the lifetime, τ, of the excited state for the recoils inside the target is then given in the following way

$$F(\tau) = \frac{v_{av}}{v_0} = \frac{1}{v_0\tau}\int_0^{\infty} v(t)e^{-\frac{t}{\tau}}dt \tag{3.5}$$

where v_{av} and v_0 are the average velocity when the γ rays were emitted and the initial velocity respectively. The velocity of the recoils will be distributed between v_0 and zero. Once the attenuation factor multiplied with v_0 is obtained, the slowing down process for the reaction and recoils of interest are simulated using Monte-Carlo techniques and known stopping powers, see e.g. Ziegler [34]. Finally the lifetime is determined by comparing the experimental data with these calculations. Typically a gate (or several gates) is set in the coincidence matrix to select the transition chain of interest. If the gate is set on a transition below the state of interest, the side-feeding has to be taken into account. The lifetime of the level in which we are interested will be affected by the lifetimes of the states feeding into this state according to the Bateman equation [35]

$$\frac{dN_i(t)}{dt} = \sum_h N_h(t)\frac{1}{\tau_h} - N_i(t)\frac{1}{\tau_i} \tag{3.6}$$

where $N_i(t)$ and $N_h(t)$ are the populations of level i and the above lying levels h respectively, at time t. The level i is not only fed by the direct feeding transition(s) from the known structure, it also has feeders from the statistical continuum with states of unknown lifetimes and possibly also from other decay chains from higher spin-states. However, if the gate is set on a transition above the state of interest,

the side-feeding does not affect the determination of the lifetime. The lifetimes of the states of interest in ^{107}Cd were too long and the velocity of the recoils was too low in order to observe a shift in the centroid of the decaying γ-ray energies. The majority of the produced recoils emitted γ rays after they had already stopped inside the target. However in some cases, depending on the lifetime of the state, the decaying γ rays were emitted during the slowing down process inside the target and depending on the velocity distribution of these γ rays the lifetime may be deduced by performing a lineshape analysis.

Lineshape Analysis

The lifetime of the state can also be obtained by determination of the γ-ray lineshape. The transition from a decaying state will be distributed over different energies, $\frac{dN}{dE}$, depending on the velocities of the recoils when the γ ray is emitted. The energy distribution is related to the velocity distribution $\frac{dN}{dv}$, according to eq. 3.4. The velocity distribution can be written as a function of the stopping power and the lifetime of the decaying state of interest in the following way

$$\frac{dN}{dv} = \frac{dN}{dt} \times \left(\frac{dv}{dt}\right)^{-1} = -\frac{N_0}{\tau} e^{-t/\tau} \times \left(\frac{dv}{dt}\right)^{-1} \tag{3.7}$$

where N_0 is the initial population of the decaying level. Using the known stopping power of the recoils $\frac{dE}{dx} = m\frac{dv}{dt}$, the lineshape of the velocity distribution can be used to determine the lifetime. In the analysis of the ^{107}Cd experiment the code LINESHAPE [36] modified by Brandolini and Ribas [37] was used. However, as mentioned above the statistics from the slowing down process did not allow conclusive results on more than a couple of states using this technique and the results have therefore not been published. Figure 3.3 shows a lifetime analysis of the 7317 keV excited state in ^{107}Cd, by using the lineshape of the 1133 keV transition following the decay. A narrow gate is set in the E_{γ_1}-E_{γ_2} coincidence matrix on the 729 keV transition following the decay of the 5231 keV state in ^{107}Cd. The fitted lineshapes of the 1133 keV transition in the backward (138.5^o) and in the forward (41.5^o) detector angle are shown. It is obvious that clean gates with little contamination from transitions between other states are of high importance. Attempts were made to find the most clean gates, also sums of gates were tried in order to improve statistics.

3.4.2 Recoil Distance Method

A technique used to measure lifetimes of medium spin states in the order of 1-100 ps is, as mentioned above, the RDM, where the recoils escape from a thin production target and are stopped at a certain variable distance. The relative amount of nuclei that are still in a certain excited state when they are stopped depends on the target-stopper distance and the velocity, i.e. the lifetime of the state. The idea behind the RDM is illustrated in fig. 3.4.

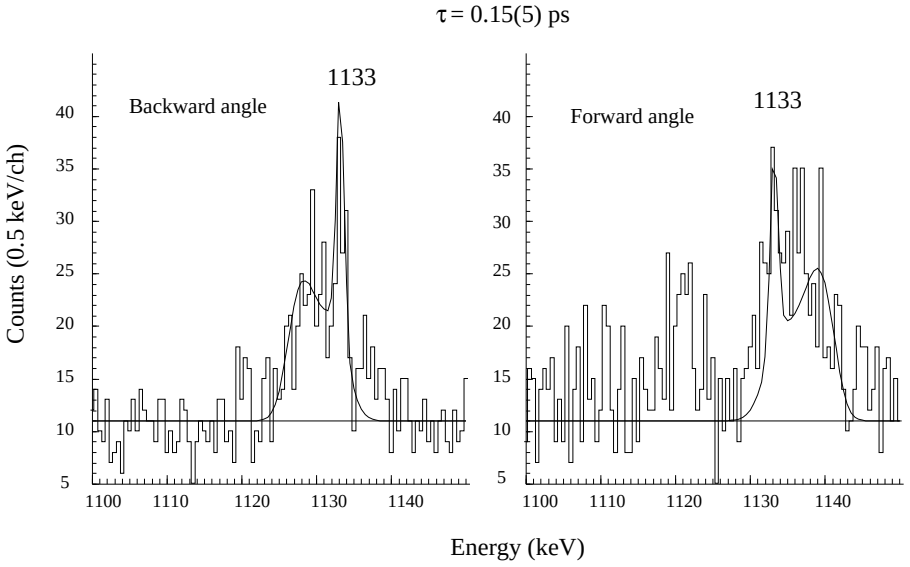

Figure 3.3: A gate is set on the 729 keV transition, decaying from the 5231 keV excited energy level in ^{107}Cd. The lineshapes of the 1133 keV transition, decaying from the 7317 keV state in the same nucleus are analysed in the backward (138.5^o) and in the forward (41.5^o) angle.

The lifetime of an excited state can be obtained using the Differential Decay Curve Method (DDCM) [38, 39]. The mean life of an excited level is given by

$$\tau \;=\; \frac{I_u}{\frac{dI_s}{dt}} \;=\; \frac{I_u}{v\frac{dI_s}{dx}} \tag{3.8}$$

where I_u and I_s are the intensities of the unshifted and shifted components of the transitions following the de-excitation of the state of interest. This formula is only valid if a gate is set on a γ ray directly feeding the state of interest. If an indirect feeder is used, the relation between the direct feeder and the de-exciting transition has to be taken into account. In the above formula, v denotes the velocity of the recoils and it is obtained by measuring the Doppler shifts of some of the strongest transitions and using eq. 3.4. The derivative in the denominator is with respect to the target-stopper distance, x. When using this method it is necessary that the E_{γ_1} - E_{γ_2} matrices are normalised with respect to the number of recoils of interest created at each target-stopper distance. A first approximation is to normalise the matrices with respect to the total number of counts at each different distance. In the ^{165}Lu experiment (**paper I**) this proved to be sufficient; it was checked that

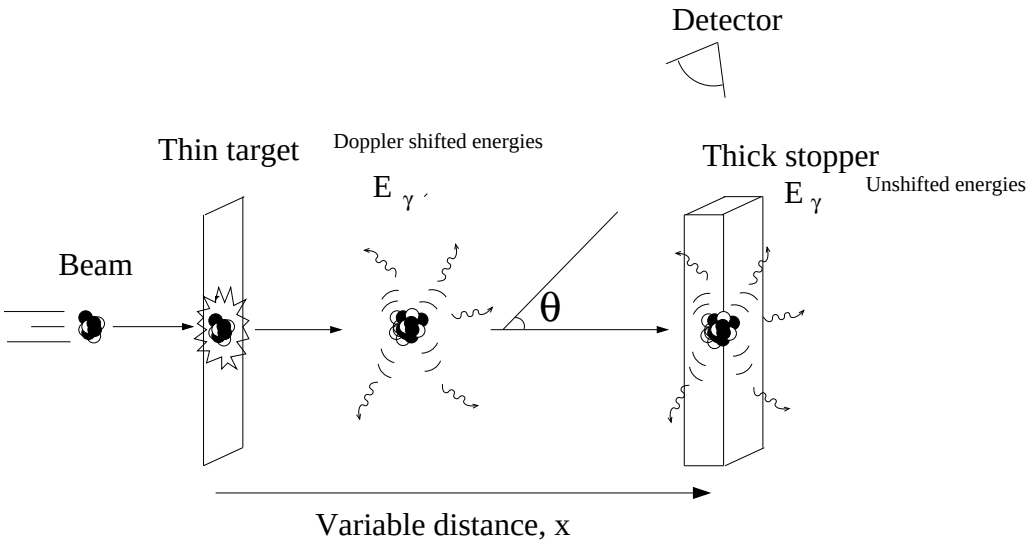

Figure 3.4: A schematic view of an RDM experiment.

this was indeed the case by measuring the intensity for the lowest transition in the nuclei of interest for all of the distances at one combination of angles and for all of the combinations of angles at one distance (taking the angular distribution for the multipole type into account). The events were sorted for each ring-ring combination and each distance, into matrices of the Cologne format [40]. In the analysis, the Cologne software packages [41, 42] were used to choose the slices and fit the intensities. In fig. 3.5 the unshifted and shifted intensities of the $23/2^- \rightarrow 19/2^-$ in the rotational band based on the $9/2^-[514]$ Nilsson orbital in ^{165}Lu at different target-stopper distances are shown. It is clearly visible how the relationship between the two intensities varies with increasing distance.

Plunger

A critical issue when using the RDM is to measure the target-stopper distance correctly. In the experiments described here this was achieved by the use of the Cologne Plunger Device (the LNL experiment) [43] and the New Yale Plunger Device (the WNSL experiment) [44] respectively. A picture of the Cologne Plunger used in combination with the GASP Ge-array can be seen in fig. 3.2. The target has to be stretched to become very flat in order to have the target and the stopper as

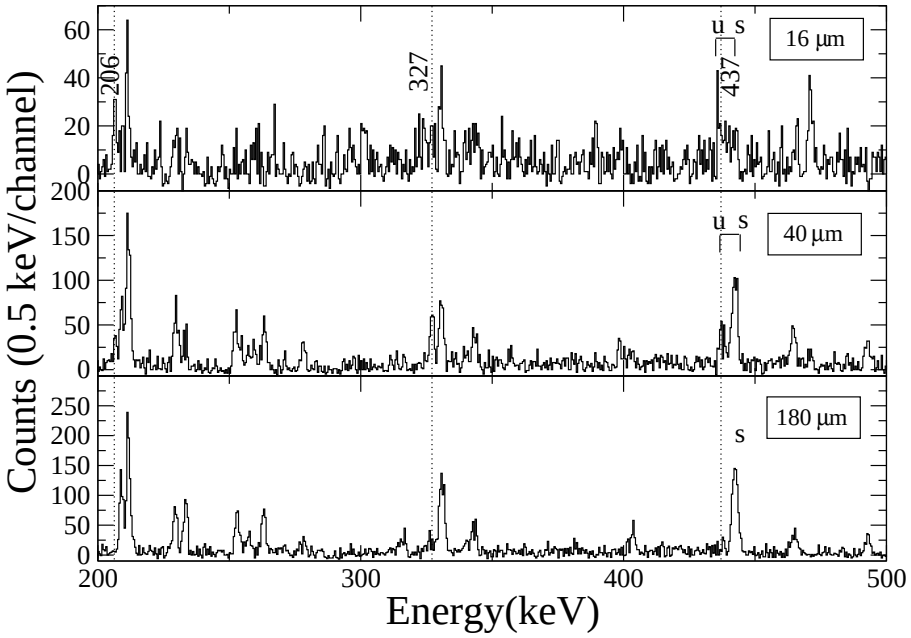

Figure 3.5: Unshifted and forward-shifted intensities of the $23/2^- \rightarrow 19/2^-$ transition of 437 keV in ^{165}Lu, see **paper I**. The spectra are obtained using a gate on the direct feeding transition of 519 keV. Both the gating and analysing angular combination is 34°-34°. The three different target-stopper distances are from top to bottom, 16, 40 and 180 μm.

parallel as possible. Both plungers use the capacitance between the target and the stopper to measure the distance correctly. The capacitance between two parallel plates is simply the area of the plates divided by their distance, $C = \epsilon_0 A/d$, where ϵ_0 is the permittivity in vacuum. The plunger devices are also equipped with a piezo-crystal, working as a feedback system to correct for fluctuations in the target position due to heating from the beam current. The distance is varied to the desired positions using a micro-meter screw and a stepping motor.

3.5 Transition probabilities

From the measured lifetimes, the transition probabilities are calculated using eq. 2.23 and from these values conclusions on the excitation mode and the shape of the nucleus can be derived in a model dependent way. When calculating the transition probability of an excited state, several aspects have to be considered. The level for which the lifetime is measured can have γ-ray decays to several different levels, which means that the branching ratio of these decays have to be taken into account. Instead of sending out a photon it is also possible for the nucleus to de-excite by *internal conversion*, which implies that the nucleus interacts with an electron in an atomic shell resulting in emission of the electron. The amount of decays via internal conversion depends on the energy difference between the states of interest, the type (electric or magnetic) and the multipole order of the transition. The multipole mixing ratios of the transitions, mainly M1/E2 mixing of $I \rightarrow I-1$ transitions and its effect on the internal conversion coefficients were also taken into account when determining the transition probability. In the case of **paper II**, where the aim was to investigate the excitation mode of the band built on the neutron $i_{13/2}$ orbital in ^{107}Cd, the ratio between the transition probability from the state of interest and the transition probability from the first excited state was examined and compared to theory. In the case of **paper I**, the aim was to investigate the shape of ^{165}Lu by measuring the lifetimes of excited states. The deformations of the different rotational bands were obtained using the equations given in section 2.5.1 and the results were compared to theoretical predictions.

Chapter 4

Summary of Papers and the Author's Contribution

The experimental results and my contribution to **papers I** and **II** are briefly discussed below. Both experiments were aimed at measuring the lifetimes of excited states using the Recoil Distance Method and the plunger technique. The first experiment was performed at Laboratori Nazionali di Legnaro in Italy and the aim was to further investigate the possible triaxiality of medium spin states in ^{165}Lu. The second experiment was performed at Yale University, New Haven, USA. Here the aim was to examine the shape evolution in the transitional nuclei ^{106,107}Cd. In the analysis, the Differential Decay Curve Method was used to extract the lifetimes. The transition probabilities of the states were derived and compared to theoretical predictions.

4.1 Paper I

The author of this thesis performed the data analysis and wrote the paper. The lifetimes of 19 excited levels in four different rotational bands in ^{165}Lu were measured for the first time. The XTU-Tandem Accelerator of Laboratori Nazionali di Legnaro was used to accelerate the ^{30}Si ions to a beam energy of 135 MeV onto a target consisting of isotopically enriched ^{139}La. After the evaporation of four neutrons, ^{165}Lu nuclei were created in highly excited states and the γ rays following the de-excitation were detected using the GASP Ge-detector array. The lifetimes of the excited levels were measured by inserting a thick stopper foil at a certain distance behind the ^{139}La target. The distance between the target and the stopper was then varied and the γ rays detected both while the recoils were still in flight and after the recoils were stopped were saved to tape. Lifetimes in the range of 1.4 - 193 ps were measured using the Differential Decay Curve Method. The reduced transition probabilities and the quadrupole moments were deduced from the lifetimes and the results compared to theoretical predictions. The comparison indicates axially sym-

metric shapes for three out of the four examined rotational bands in this nucleus. However, for the band built on the $9/2^-[514]$ there is experimental support for a triaxial deformation.

4.2 Paper II

The author participated in the experiment resulting in **paper II**. Almost the entire paper was written by the author who also performed the data analysis. In this paper, lifetimes in ^{107}Cd are reported. The beam of ^{12}C ions was delivered by the Wright Nuclear Structure Laboratory Yale Tandem Accelerator at a beam energy of 60 MeV. The target consisted of an isotopically enriched foil of ^{98}Mo ions and after compound nucleus formation followed by evaporation of three neutrons, the nuclei of interest were created. The γ rays following the de-excitation of the nucleus were detected using the SPEEDY Ge-detector array. Also in this experiment the plunger technique was used and lifetimes of two excited states in the band built on the $i_{13/2}$ neutron orbit were measured using the Differential Decay Curve Method. The reduced transition probabilities were deduced and the mode of excitation for these levels is discussed by comparisons with theoretical prediction. There is need for further lifetime measurements of higher spin states, or comparisons to the transition probabilities in the even-even core of ^{106}Cd, before conclusive arguments can be drawn regarding the excitation mode of the levels built on the neutron $i_{13/2}$ orbital in ^{107}Cd.

Acknowledgements

First of all I would like to thank Bo Cederwall for his guidance and support. I thank Paddy Regan for giving me the opportunity to discover the world of nuclear physics and to experience the British islands. I also wish to thank Zsolt Podolyák for his intelligent supervision, Stephen Ashley for his persistence, and the rest of the Surrey group for making my stay in England so enjoyable by being as fun-loving and friendly as they are. At the department at KTH I would like to thank my colleagues, Baharak, Micke, Anton, Daniel, Ela and Shufang for their interesting discussions concerning anything you could possibly think of. I'm also ever so thankful to the senior staff members, Lars-Olov Norlin, Ramon Wyss and Andras Kerek who are always willing to answer any questions, a special thanks to Arne Johnson and Roberto Liotta for proof-reading and improving this thesis. Thanks also to the Reactor Department for their friendship and especially Torbjörn for his excellent way of explaining physics concepts and helping me to choose the correct path in the jungle of software. Finally I would like to thank Seehuhn for existing, my family for their love and Nils for never giving up on me. Last but not least I would like to thank ^{165}Lu and ^{107}Cd for assembling themselves during such short periods of time in the suburbs of Padova and in the small American town of New Haven, without you, none of this would have been possible.

And this one goes out to all of you elementary particles out there!

Bibliography

[1] M. G. Mayer. *Phys. Rev.*, 75:1969, 1949.

[2] J. H. D. Jensen O. Haxel and H. E. Suess. *Phys. Rev.*, 75:1766, 1949.

[3] A. Bohr. *Kgl. Danske Videnskab. Selskab, Mat.-fys. Medd.*, 26:No. 14, 1952.

[4] A. Bohr and B. R. Mottelson. *Kgl. Danske Videnskab. Selskab, Mat.-fys. Medd.*, 27:No. 16, 1953.

[5] A. Arima and F. Iachello. Interacting boson model of collective states. *Ann. Phys. (N.Y.)*, 99:253, 1976.

[6] K. L. G. Heyde. *The Nuclear Shell Model*. Berlin Heidelberg: Springer-Verlag, 2 edition, 1994.

[7] S. G. Nilsson. *Kgl. Danske Videnskab. Selskab, Mat.-fys. Medd.*, 29:No. 16, 1955.

[8] D. R. Inglis. *Phys. Rev.*, 96:1059, 1954.

[9] R. Bengtsson and S. Frauendorf. *Nucl. Phys. A*, 327:139, 1979.

[10] S. Frauendorf. *Nucl. Phys. A*, 3557:259c, 1993.

[11] `http://en.wikipedia.org/wiki/Liquid_drop_model`.

[12] J. Reinwater. *Phys. Rev.*, 79:432, 1950.

[13] A. Bohr. *Phys. Rev*, 81:331, 1951.

[14] A. Bohr and B. Mottelson. *Phys. Rev.*, 90:717, 1953.

[15] P. Ring and P. Schuck. *The Nuclear Many-Body Problem*. New York Inc.: Springer-Verlag, 1980.

[16] D. L. Hill and J. A. Wheeler. *Phys. Rev.*, 89:1102, 1953.

[17] K. E. G. Löbner *et* al. *Nuclear Data Tables A*, 7:495, 1970.

[18] V. M. Strutinsky. *Nucl. Phys. A*, 95:420, 1967.

[19] A. Bohr and B. Mottelson. *Nuclear Structure VolumeII: Nuclear Deformations*. Singapore: World Scientific, 2nd edition, 1998.

[20] P. Petkov *et* al. *Nucl. Phys. A*, 640:239, 1998.

[21] R. F. Casten and D. Warner. *Rev. Mod. Phys.*, 60:389, 1988.

[22] P. H. Regan. *Phys. Rev. Lett.*, 90:152502, 2003.

[23] `http://www.gsi.de`.

[24] `http://www.ganil.fr/spiral2`.

[25] `http://www.riken.go.se`.

[26] `http://www.phy.ornl.gov/hribf`.

[27] `http://www.nscl.msu.edu/ria`.

[28] `http://www.triumf.ca/isac/isac_home.html`.

[29] K. S. Krane. *Introductory Nuclear Physics*. John Wiley & Sons, Inc., 1998.

[30] G. F. Knoll. *Radiation Detection and Measurement*. John Wiley & Sons, Inc., 3rd edition, 2000.

[31] R. Krücken. *Proc. Int. Symp. on Advances in Nuclear Physics (Bucharest, Romania, 1999)*. Singapore: World Scientific, 2000.

[32] D. Bazzacco. *Proceedings of the International Conference on Nuclear Structure at High Angular Momentum (Ottawa, Canada, 1992)*. Chalk River Report No. AECL 10613, 1992.

[33] J. B. Marlon and D. M. Patter. *Nuclear Research with Low Energy Accelerators*. Academic Press, New York, 1967.

[34] J. F. Ziegler. *Handbook of Stopping Cross-sections For Energetic Ions in All Elements*. Pergamon, New York, 1980.

[35] H. Bateman. *Proc. Camb. Phys. Soc.*, 15:423, 1910.

[36] J. C. Wells and N. R. Johnson. *Report No. ORNL-6689*, page 44, 1991.

[37] F. Brandolini and R. V. Ribas. *Nucl. Instr. and Methods in Phys. Res. A*, 417:150, 1998.

[38] A. Dewald *et* al. *Z. Phys. A*, 334:163, 1989.

[39] G. Böhm. *Nucl. Instr. and Methods in Phys. Res.*, page 248, 1993.

[40] http://www.ikp.uni-koeln.de.

[41] J. Theuerkauf. Tv. unpublished, http://www.ikp.uni-koeln.de.

[42] B. Saha. Napatau. unpublished, http://www.ikp.uni-koeln.de.

[43] A. Dewald *et* al. *Proceedings of the Seminar on Nuclear Physics with Radioactive Ion Beam and High Spin Nuclear Structure, (Lanzhou, China).* Atomic Energy Press, Lanzhou, China, 1998.

[44] R. Krücken. *J. Res. Natl. Stand. Technol.*, 105:53, 2000.